Extreme Helicity and Intense Convective Towers in Hurricane Bonnie

John Molinari[1] and David Vollaro
Department of Earth and Atmospheric Sciences
University at Albany, SUNY

Submitted to *Monthly Weather Review*
October 10, 2007

Revised
February 27, 2008

[1]Corresponding author address:
Department of Earth and Atmospheric Sciences, ES-225
University at Albany/SUNY
Albany, NY 12222.
molinari@atmos.albany.edu

Abstract

Helicity was calculated in Hurricane Bonnie (1998) using tropospheric-deep dropsonde soundings from the Convection and Moisture Experiment conducted by NASA. Large helicity existed downshear of the storm center with respect to the ambient vertical wind shear. It was associated with veering, semi-circular hodographs created by strong, vortex-scale, radial-vertical flow induced by the shear. The most extreme values of helicity, among the largest ever reported in the literature, occurred in the vicinity of deep convective cells in the downshear-left quadrant. These cells reached as high as 17.5 km and displayed the temporal and spatial scales of supercells.

Convective available potential energy (CAPE) averaged 861 J kg^{-1} downshear, but only about one third as large upshear. The soundings nearest the deep cells were evaluated using two empirical supercell parameters that make use of CAPE, helicity, and/or shear. These parameters supported the possible existence of supercells as a consequence of the exceptional helicity combined with moderate but sufficient CAPE.

Ambient vertical wind shear exceeded 12 ms^{-1} for 30 hours, yet the hurricane maintained 50 ms^{-1} maximum winds. It is hypothesized that the long-lived convective cells enabled the storm to resist the negative impact of the shear.

Supercells in large-helicity, curved-hodograph environments appear to provide a useful conceptual model for intense convection in the hurricane core. Helicity calculations might also give some insight into the behavior of vortical hot towers, which share some characteristics with supercells.

1. Introduction

The concept of helicity has proven useful for the prediction of supercells, which contain large helicity and relatively long lifetimes. Lilly (1986) argued that large helicity suppresses the inertial range energy cascade, so that helical cells resist dissipation and survive longer than ordinary thunderstorms. Lilly (1986) and Wu et al. (1992) have shown that supercells gain substantial helicity from their environment. As a result, environmental helicity calculated from soundings (Davies-Jones et al. 1990) has been used to determine the likelihood of supercell occurrence in middle latitudes. Brooks and Wilhelmson (1993) showed that when environmental helicity was high, their simulated storms evolved in such a way that buoyancy and vertical pressure gradient force acted in concert. This allowed greater vertical penetration of cells than implied by buoyancy alone. Levich and Tzvetkov (1984) noted that mean-square helicity tends to organize itself on larger scales, somewhat analogous to an upscale energy cascade (Lilly 1986).

It is not obvious that concepts tested in midlatitude supercells should be relevant in tropical cyclones. The latter generally have larger ambient vertical vorticity, smaller vertical wind shear (e.g., Hanley et al. 2001), and smaller convective available potential energy (CAPE; Jorgensen et al. 1985; Bogner et al. 2000) than the environments of middle latitude severe weather. Recently, Montgomery et al. (2006) described "vortical hot towers" (VHTs) occurring in their numerical simulation of tropical cyclone formation. Because local vertical wind shear was relatively small in Montgomery et al.'s (2006) idealized simulations, the VHTs were likely not supercells. Nevertheless, they contained tropospheric-deep updrafts coinciding with large values of the vertical component of vorticity and lifetimes on the order of an hour or more, and thus had several traits in common with supercells. Montgomery et al. (2006) described tropical

cyclone formation in terms of an upscale organization of these VHTs, possibly analogous to the arguments of Levich and Tzvetkov (1984). Given the similarities of VHTs to supercells, there is reason to believe that helicity calculations might provide insight into the behavior of strong convection in tropical cyclones.

Further support was provided by Stiegler and Fujita (1982), who argued that intense convection after tropical cyclone landfall occurred in supercell-like storms. Novlan and Gray (1974) noted the large vertical shears after landfall in the vicinity of tropical cyclone-spawned tornadoes. McCaul (1987, 1991) examined nearby soundings to such tornadoes and found high environmental helicity values. McCaul and Weisman (1996) simulated supercell formation using characteristic soundings after tropical cyclone landfall. The resultant supercells resembled those in middle latitude severe convection, but had smaller vertical extent, consistent with shallower layers of vertical wind shear and CAPE. The McCaul and Weisman (1996) simulations showed that midlatitude severe weather concepts were directly transferable to convection in tropical cyclones.

The large helicity in the soundings of McCaul (1987, 1991) arose from strong low-level shear associated both with frictional decay after landfall and with baroclinicity. In tropical cyclones over water, such circumstances are much less likely. Bogner et al. (2000) examined helicity in 130 dropsondes from tropical cyclones over water. Bogner et al. found that maximum helicity values were about half the typical value found by McCaul (1991) in tropical cyclones after landfall. Most often helicity fell below the numerical criteria for supercells in middle latitudes (see section 5a).

Nevertheless, tropical cyclones over water are known to have occasional long-lasting, intense convective cells (Gentry et al. 1970; Heymsfield et al. 2006). Black and Marks (1987)

used the term "supercell" to describe such events. Several such cells have been studied in Hurricane Bonnie (1998) by Heymsfield et al. (2001). In this paper the helicity distribution in Hurricane Bonnie will be examined. Extreme values of helicity, larger than in severe middle latitude convection, will be shown to occur in the vicinity of the intense cells. The reasons for these large values, and their role in the behavior of the storm, will be discussed.

2. Applications of Helicity to Tropical Cyclones

Total helicity is given by the scalar product of the three-dimensional velocity and vorticity vectors. In midlatitude severe weather applications, the terms involving the vertical motion in both the velocity and vorticity vectors are usually neglected, because helicity is evaluated from environmental soundings (i.e., away from individual cells where such terms might be large). The resulting expression for total helicity can then be written (Lilly 1986):

$$H_{TOT} = \boldsymbol{v} \cdot \left(\boldsymbol{k} \times \frac{\partial \boldsymbol{v}}{\partial z} \right) = \boldsymbol{k} \cdot \left(\frac{\partial \boldsymbol{v}}{\partial z} \times \boldsymbol{v} \right) \qquad (1)$$

where $\boldsymbol{k}$ is the vertical unit vector and $\boldsymbol{v}$ is the horizontal velocity vector. The neglect of the $w\zeta$ term required to obtain Eq 1 must be justified for the tropical cyclone environment. The following assumptions are made: (i) w = 2-3 ms^{-1} averaged over the lowest 3 km, consistent with typical lower tropospheric vertical velocities away from active cells (Black et al. 1996); and (ii) ζ = 2 X 10^{-3} s^{-1} over a 3-km depth, equivalent to tangential velocity of 50 ms^{-1} at a radius of maximum winds of 25 km. Under these circumstances, the vertical integral of $w\zeta$ over 3 km is only 12-18 m^2 s^{-2}. This value is an order of magnitude smaller than calculated helicity values in this study (see section 5a). Outside the core, smaller ambient vorticity further reduces the

vertical helicity component. The neglect of this term appears to be justified, even in tropical cyclones.

Lilly (1986) showed that a "clockwise-turning" (veering) hodograph produces large positive helicity. Such a hodograph comes closest to having the velocity vector perpendicular to the shear vector at every level, maximizing the cross product in the second part of Eq 1. Curved hodographs produce the most efficient extraction of helicity from the environment (Droegemeier et al. 1993; Wu et al. 1992).

It is the tropical cyclone itself that provides the environmental helicity for individual cells within it. For a vortex without radial winds, $H_{TOT} = 0$ even if tangential wind varies strongly with height, because the velocity and vertical wind shear vectors are parallel or antiparallel, making the cross product equal to zero in Eq. 1. Consider an idealized axisymmetric, stationary tropical cyclone with friction-induced veering winds in the boundary layer, and gradient balance otherwise. The only helicity beneath the outflow layer in such a storm lies in the boundary layer, where the veering wind makes it positive. To the extent that tropical cyclones in nature resemble the above description, large helicity is not guaranteed. It is perhaps for this reason that Bogner et al.'s (2000) values in tropical cyclones over water did not commonly reach levels indicative of supercell convection.

In cylindrical coordinates, Eq. 1 can be written:

$$H_{TOT} = -v_r \frac{\partial v_\lambda}{\partial z} + v_\lambda \frac{\partial v_r}{\partial z} \qquad (2)$$

where v_r and v_λ and are the radial and tangential velocity components, respectively. Tangential velocity is large and positive almost everywhere in a tropical cyclone. As a result, the largest helicity might be expected in layers where the radial wind increases upward.

Total helicity is not directly relevant to the growth of individual cells within a tropical cyclone. Instead, Davies-Jones et al. (1990) showed that helicity must be calculated relative to the moving cell. In addition, Davies-Jones et al. (1990; see also Davies-Jones 1984) argued that the vertical integral of cell-relative environmental helicity (SREH) provided a useful supercell forecast variable. [Cell-relative helicity is called "storm-relative" in midlatitude severe weather literature, but the former term will be used here in order to avoid confusion with the wind relative to the moving tropical cyclone, also called "storm-relative".] The variable SREH is given (Davies-Jones et al. 1990) by

$$SREH = \int_o^h \left[(\boldsymbol{v} - \boldsymbol{c}) \cdot \left(\boldsymbol{k} \times \frac{\partial \boldsymbol{v}}{\partial z} \right) \right] dz \qquad (3)$$

where $\boldsymbol{c}$ is the vector cell motion and h is most often taken as 1, 3, or 6 km. Various numerical studies (e.g., Droegemeier et al. 1993; Weisman and Rotunno 2000) and observational studies (Brandes et al. 1988; Davies-Jones et al. 1990; Johns and Doswell 1992; Kerr and Darkow 1996; Rasmussen and Blanchard 1998; Thompson et al. 2003) have shown the utility of SREH in supercell and tornado prediction in middle latitude convection. SREH will form the basis for this study. Calculation procedures are described in the following section.

3. Data Sources and calculation methods

SREH (hereafter "helicity") will be calculated from Eq. 3 using dropsonde soundings taken during the NASA Convection and Moisture Experiment (CAMEX-3; Kakar et al. 2006). A total of 21 dropsondes were released in Hurricane Bonnie from a DC-8 aircraft at about the 250-hPa level during 23-26 August 1998. Winds in the soundings were first interpolated linearly with height to 100 m levels. Ten soundings did not contain a surface wind, and two of those

were missing a wind at the 100 m height as well. For those soundings, the helicity in the missing 100 or 200 m near the surface was assumed to be equal to the mean in the remainder of the lowest 1-km layer. This conservative assumption avoided downward extrapolation of the wind. The influence of this assumption on helicity is small, because the missing layers make up only 3-7% of the depth of the 3 and 6 km layers, and even less for deeper layers.

If winds were missing over more than 200 m at the surface, or were missing over a layer greater than or equal to 1.5 km in the remainder of a sounding, the sounding was not used. Three soundings were omitted for that reason. Finally, only sondes within 350 km of the center were analyzed. This left 17 soundings for which helicity was calculated. The first 6 were released between 1845 UTC and 2136 UTC 23 August; a second set of 7 were released between 2330 UTC 24 August and 0153 UTC 25 August; and the final set of 4 between 1220 UTC and 1535 UTC 26 August.

Helicity has proven to be sensitive to the choice of cell motion (e.g., Ramsay and Doswell 2005). The most accurate measure comes when supercells are tracked on radar. In the current study, radar data were unavailable. Instead the method of Bunkers et al. (2000) will be used, with the modification proposed by Ramsay and Doswell (2005). This method assumes that cell motion contains a component equal to the mean motion over the layer from the surface to 8 km, plus a component 90º clockwise of the 0-6 km layer vertical wind shear. Ramsay and Doswell (2005) showed that this method produced relatively small errors (median 2.9 ms^{-1}) in cell motion estimates. Cell motion will also be estimated using simply the mean wind over 6 km, but only for comparison with the results of McCaul (1991). Other methods are evaluated in the Appendix. The Appendix shows that, even though quantitative differences exist, the

azimuthal helicity distribution and the presence of extreme helicity were insensitive to the cell motion estimate.

CAPE was also calculated in this study. CAPE calculations required insertion of temperature values above the flight level using gridded analyses from the European Centre for Medium-Range Weather Forecasting (ECMWF). For two soundings the ECMWF values were too cold, producing superadiabatic layers in the soundings above flight level. In order to reduce this problem, potential temperature in all soundings was interpolated linearly between the first (i.e., highest) level of the sonde and the 150 hPa level in the gridded analyses. The sounding temperature above flight level was calculated from this interpolated potential temperature. CAPE was significantly (and appropriately) reduced in one sounding as a result of this correction. CAPE was virtually unaffected in the remaining soundings, either because the gridded analysis temperature closely matched the dropsonde, or because the CAPE contribution above flight level was negligible.

Two calculations of vertical wind shear are relevant. System-wide shear from 850 hPa to 200 hPa makes use of azimuthally-averaged Cartesian wind components (Corbosiero and Molinari 2002), thus removing the shear of the mean vortex and retaining only the cross-storm component. This system-wide shear is calculated from gridded ECMWF analyses over 500 km of radius. The system-wide (hereafter "ambient") shear strongly influences the asymmetry of the convection with respect to the tropical cyclone center (e.g., Black et al. 2002; Corbosiero and Molinari 2002, 2003; Rogers et al. 2003; Chen et al. 2006). In contrast, individual cells respond to the *local* shear in each sounding that includes the contribution of the mean vortex. Following standard practice in middle latitude severe weather studies, the local shear will be taken as the vector difference between the 5500-6000 m mean wind and the 0-500 m mean wind. The

maximum local shear in this study exceeds the ambient value by a factor of 3-5. The terms "upshear" and "downshear" will always refer to the side of the storm with respect to the ambient shear vector.

In some figures, the location of the mean wind and local vertical shear vectors from dropsondes will be rotated azimuthally to orient them with the direction of the ambient shear. This requires a comparable rotation of the vector directions to maintain the relationship between the mean wind and wind shear.

4. History of Hurricane Bonnie

a. Track and intensity

The history of Hurricane Bonnie is described by Heymsfield et al. (2001) and Rogers et al. (2003). Figure 1 shows the minimum central pressure and maximum surface winds from the Best Track produced by the National Hurricane Center, plus an estimate of the 850-200 hPa ambient vertical wind shear. The storm began to intensify rapidly late on 21 August in the presence of weak vertical wind shear and warm ocean temperatures. During 23 August, wind shear significantly increased, reaching more than 12 ms^{-1} by 0000 UTC 24 August. Despite this dramatic increase in shear, the storm continued to intensify. The lowest minimum central pressure was reached near 0000 UTC 24 August. Vertical wind shear remained above 12 ms^{-1} for 30 hours, yet the maximum Best Track winds remained at 50 ms^{-1} and the minimum central pressure rose only slightly. Late on 25 August, vertical wind shear returned to small values. The gray strips in Figure 1 indicate the periods of dropsonde releases in CAMEX-3. The first two sets of dropsondes were released in the presence of large ambient wind shear, and the third during small ambient wind shear.

Braun et al. (2006; their Figure 1) showed three alternative measures of 850-200 hPa vertical wind shear in Hurricane Bonnie, but for magnitude only. Although details differ, all three of their estimates show vertical shear magnitude exceeding 8 m s^{-1} (and as large as 15 m s^{-1}) during 24-25 August, and decreasing rapidly prior to the third release on 26 August.

Sea surface temperatures increased by about 1ºC along the track of the storm from late on 21 August until early on 25 August (Heymsfield et al. 2001), reaching a maximum of 30.5ºC at the latter time. The ability of the storm to resist the large wind shear must relate in part to the warm water. A second factor in the storm's resistance to shear will be proposed in this paper.

Using GOES Rapid Scan images late on 23 August, Heymsfield et al. (2001; their Figure 3) showed the existence of several intense cells that formed southeast of the center (downshear), intensified as they moved cyclonically around the eye, and dissipated upshear. Intense cells also occurred downshear of the center late on the 24th and early on the 25th, during the second release of dropsondes. This study will focus on these two periods of intense convection and large vertical wind shear on 23-25 August. The helicity values on 26 August, after the large ambient vertical shear subsided, will be shown for comparison.

b. Previous studies of Hurricane Bonnie

Hurricane Bonnie is one of the most studied storms of recent years, primarily owing to the data collected in CAMEX-3. Numerical simulations were carried out by Rogers et al. (2003), Zhu et al. (2004), Braun et al. (2006), and Cram et al. (2007). High-resolution simulations are frequently preceded by coarser-resolution simulations in order to provide a realistic storm structure prior to the insertion of an inner fine grid. Rogers et al. (2003) began high resolution 1.67 km inner grids at 0000 UTC 25 August, and thus omitted most of the period of interest in this paper. During their coarser mesh simulation, the storm intensified unrealistically.

Nevertheless, after 0000 UTC 25 August, Rogers et al. simulated realistic asymmetries in convection, and the subsequent increase in symmetry with time as the vertical wind shear decreased. They showed clear relationships between vertical wind shear within 200 km of the center in the simulation, tilt of the vortex downshear, and the amplitude of azimuthal wavenumber 1 in the simulated reflectivity field. Early on 25 August in the presence of large vertical wind shear, their simulated convective features in the storm core were almost circular, consistent with observations. On 26 August when vertical shear was small, their simulated convection was far more filamented. Possible reasons for this behavior will be addressed in the current paper. Rogers et al. (2003) did not calculate helicity, but they did show a clockwise-turning hodograph in the simulated environmental flow.

Zhu et al. (2004) used a 4-km inner mesh over 5 days beginning 1200 UTC 22 August. Their simulation covered the entire period studied in this paper. They noted the similarity between their simulated reflectivity and that shown by the EDOP instrument (Heymsfield et al. 1996) late on 23 August. They did not, however, describe features in the simulation similar to the repeated occurrence of deep cells shown by Heymsfield et al. (2001). They investigated the reasons for the intensification of Hurricane Bonnie on 23 August during the period of large wind shear. They attributed the intensification to two circumstances: strong southeasterly inflow in the lower troposphere east of the center, and strong northwesterly inflow in the upper troposphere northwest of the center. The combination produced intense convection downshear and suppressed convection upshear. Zhu et al. (2004) argued that subsidence within the eye was enhanced by upper tropospheric convergence upshear, thereby maintaining the warm core against the vertical wind shear. Heymsfield et al. (2001) provided an alternative hypothesis: that eye subsidence associated with overshooting convection downshear helped to maintain the storm

against the vertical shear. The common thread in these arguments is the role of the shear-induced circulation in opposing the impact of the shear.

Braun et al. (2006) used a 2-km inner mesh for 36 h beginning 1200 UTC 22 August. They noted the presence in their simulation of deep, vertically coherent columns with strong updrafts coincident with large cyclonic vorticity. These characteristics resemble those of shallow supercells, and of the VHTs described by Montgomery et al. (2006). The cells formed downtilt-right and dissipated downtilt-left and covered less than half of the circulation. Braun et al. (2006) thus simulated some aspects of the intense cells described by Heymsfield et al. (2001). Cram et al (2007) examined the Braun et al. (2006) simulations at 3-minute intervals for the period from 0900-1400 UTC 23 August. Cram et al. (2007) calculated numerous trajectories of air that ended up in the eye or eyewall. They described in detail the mixing that arises from vertical wind shear.

None of the numerical studies considered the influence of helicity. Although the current study examines a set of only 17 dropsondes, each sonde provides direct measurements over a deep layer. The sondes are also distributed spatially over almost the entire azimuthal and radial extent of the storm, including the vicinity of the intense convective cells observed on 23-25 August.

5. Results

a. Helicity values

Figure 2 shows the locations of the dropsondes in Hurricane Bonnie during the first two observation periods, when vertical wind shear was large. The positions of the sondes are plotted with respect to the moving center, and have been rotated with respect to the ambient vertical

wind shear following Corbosiero and Molinari (2002). The downshear direction is toward the right side of the figure. Two helicity values are shown for each sonde. The top value represents the 0-6 km layer, and the lower value the 0-3 km layer. Finally, the mean wind vector over the lowest 6 km is shown using wind barbs.

The helicity distribution in Figure 2 related closely to the direction of the ambient vertical wind shear. Downshear values generally exceeded those from upshear, and the largest values occurred in the downshear-left quadrant. Some downshear helicity values far surpassed those needed for multiple tornado outbreaks in middle latitudes, as well as those in close proximity to hurricane landfall tornadoes. This will be discussed further below. Figure 2 also shows that the radial extent of hurricane-force winds was greater downshear.

Figure 3 shows the dropsondes in the same configuration as Figure 2, but with 0-6 km vertical wind shear vectors and CAPE values. The vertical shear vectors support the earlier remarks based on Eq 2: the largest helicity (sondes D2, D9 and D10) generally coincided with the local vertical shear vector directed outward from the center, i.e., exhibiting large increase of radial wind with height, with a magnitude of 32-45 m s^{-1}. Local vertical shear values were much smaller upshear.

CAPE values in Figure 3 also varied with the direction of the ambient shear vector. Downshear values ranged from 218 to 1556 J kg^{-1}, with a mean of 861 J kg^{-1}. All upshear values fell below 1000 J kg^{-1}, with a mean value of 291 J kg^{-1}.

Figure 4 shows an infrared satellite image of Hurricane Bonnie at 2200 UTC 23 August, during the period shown by Heymsfield et al. (2001) to have frequent intense cells. The wind barbs represent the mean wind over the lowest 6 km. Also shown are 0-6 km helicity values for the six dropsondes released on 23 August. These are plotted with respect to the moving center,

but not rotated with respect to the vertical wind shear, which is from the northwest at this time (Figure 1). An intense cell existed northeast of the center (left of shear), and a second cell was developing southeast of the center (downshear). The two dropsondes with large helicity (D2 at 1859 UTC 23 August and D5 at 2119 UTC 23 August) were released on either side of the region where the most intense convection developed throughout the period. The remaining sondes fell well outside the strong cells and contained much lower helicity values.

As noted earlier, Heymsfield et al. (2001) described the evolution of 5 cells between 1800 and 2200 UTC 23 August. Each cell formed upwind of an existing cell as in Figure 4. They rapidly intensified as they moved azimuthally and slightly outward from the center, and dissipated upshear. The cells lasted about 90-120 minutes, reached altitudes as high as 17.5 km with cloud top temperatures often below -80ºC (see Figure 4), and exhibited small spatial scales (20-25 km) even on infrared satellite images. These cells displayed the temporal and spatial scales of supercells. The "back-building" behavior described above (e.g., Bluestein and Jain 1985) effectively extended the eyewall from half open to more than three-quarters closed over four hours (see Figure 3 of Heymsfield et al. 2001).

Late on 24 August, localized individual convective cells displayed similar behavior to those on 23 August. Early on 25 August, the cloud distribution became far more asymmetric with respect to the storm center. Figure 5 shows infrared satellite images at 0100, 0200, and 0300 UTC. Helicity values and mean winds are shown in Figure 5a. At 0100 UTC, a cell was beginning to grow just east of the center (downshear at this time; see Figure 1). During the following two hours (Figures 5b, 5c), the cell grew dramatically. Sondes D9 and D10 contained the largest helicity. Cell growth occurred in the same region of the storm as these two large helicity values. Helicity values were also elevated in the region upwind of the deepest cells

(sondes D12 and D13). The remaining sondes on 24-25 August (Figure 5a) were located outside of the deep convection and generally contained much smaller helicity values. Taken together, Figures 2, 4, and 5 show that the largest helicity occurred in the four soundings closest to the deep cells on the two days (D2, D5, D9, and D10).

Table 1 gives the typical values of helicity over a 3-km layer from operational analyses in middle latitude severe weather (Thompson et al. 2003). Included are mean values for three types of convection: without supercells, with non-tornadic supercells, and with significant tornadic events. Table 1 compares Thompson et al.'s (2003) helicity values with the upshear mean and downshear mean values over 3, 6, and 12 km in this study, as well as with the mean over the four sondes closest to the deep convection. In addition, the magnitude of 0-6 km vertical wind shear is shown for the same cases.

The mean upshear helicity in Hurricane Bonnie is similar to the nontornadic supercell values of Thompson et al. (2003). The mean downshear helicity is nearly three times as large, and more than double the value from the strong tornadic events of Thompson et al. (2003). In the four near-convection soundings in the hurricane, the mean helicity reaches extreme values that are three times the strong tornadic supercell values in middle latitudes. Downshear sondes were released at a mean radius of 192 km, upshear sondes at 177 km. As a result, the differences between upshear and downshear sondes did not relate to a notable variation in their mean distance from the center.

The helicity values in Table 1 reach even greater extremes over 6 km and 12 km layers, with mean values as large as 1628 $m^2 s^{-2}$ for soundings nearest the deep convection. The local vertical shear magnitudes have comparable variation. Upshear of the center, shear is equivalent to minimal supercell values in middle latitudes. Mean local shear downshear of the center and

near the deep convection exceeds 30 ms^{-1}, larger than in all of Thompson et al.'s (2003) composites.

The final column in Table 1 shows the mean helicity and local vertical shear values in Hurricane Bonnie over the four dropsondes released on 26 August, after ambient vertical wind shear had decreased dramatically (Figure 1). The mean helicity on that day also decreased, especially over deeper layers. This suggests that the elevated values on previous days were associated in some manner with the large ambient vertical wind shear. This will be addressed in Section 5b.

A second comparison to midlatitude values arises from the work of Kerr and Darkow (1996), who examined 0-3 km helicity in 184 near-tornado soundings. All but two of the 184 values fell below the mean 0-3 km near-convection helicity in Table 1. Kerr and Darkow's (1996) maximum helicity of 850 m^2 s^{-2} fell well short of the maximum value of 1303 m^2 s^{-2} (sonde D10; see Figure 2) over a comparable layer in Hurricane Bonnie.

Table 2 compares helicity in Hurricane Bonnie to mean values after hurricane landfall in any storm that contained at least one tornado, and also to values from soundings close to tornadoes after landfall (each from McCaul 1991). Following McCaul (1991), the cell motion estimate in Eq 3 was taken as the mean wind over the lowest 6 km. This creates a substantial underestimate of the helicity (McCaul 1991; see Appendix in this paper), but is required for a meaningful comparison. The downshear helicity values in this study exceeded the mean value close to tornadoes after tropical cyclone landfall, especially over the deeper layers. Helicity in Hurricane Bonnie was even greater in the soundings nearest the deep cells.

b. Properties of large-helicity soundings

Figure 6 shows Skew T-log p diagrams of the four soundings with largest helicity. Sonde D2 (Figure 6a) was released just inside of the eyewall radius at an azimuth where the eyewall was open, at about 1900 UTC 23 August (not shown). The small CAPE was not surprising at this location. Largely unsaturated air existed above the boundary layer, with lowest relative humidity near 600 hPa. No evidence of a melting layer was present in the temperature profile, suggesting that little or no precipitation was falling. Clockwise turning of the wind with height was strongest in the boundary layer and outflow layer.

Sonde D5 (Figure 6b) was released near the time of Figure 4. It fell within a strong lateral gradient of brightness temperature, with a very intense cell radially inward and only low clouds further out. The presence of a deep nearly saturated layer and a narrow isothermal layer at the melting level suggested modest non-convective precipitation. The nearly moist adiabatic sounding contained small CAPE. The presence of saturation in a well-mixed layer near the surface probably represented an artifact of instrument wetting (e.g., Bogner et al. 2000), but CAPE was so small that this error had little impact.

Sondes D9 and D10 (Figures 6c and 6d, respectively) were released further from the center, but contained winds almost as strong as the previous two, owing to the extension of hurricane-force winds downshear in the storm (Figure 2). Both were released in a region of cloud-top temperatures below -55ºC, but not within active cells. D9 contained the clearest indication of melting of precipitation. These soundings were considerably more unstable than the previous two, and strong cells developed near their locations within two hours of their release (Figure 5b,c).

Figure 7 shows hodographs for the four soundings in Figure 6. Clockwise turning occurred through a deep layer in each sounding. They resembled the tornadic sounding after

hurricane landfall shown by McCaul (1987), except that lower tropospheric wind speeds were much larger. The product of large horizontal winds, large vertical shear, and clockwise turning produced exceptional helicity by the reasoning of section 2. Other soundings with relatively large helicity (not shown) also displayed a clockwise-turning hodograph; no soundings in the hurricane contained a "straight-line" hodograph (e.g., Weisman and Klemp 1982).

One of the striking aspects of Figure 7 and Table 2 is the depth of the large helicity. Figure 8 shows a vertical profile of helicity in 1-km layers for the mean upshear and downshear soundings. Upshear, the largest helicity was associated with veering winds in the boundary layer. Helicity quickly decreased to zero in the layer centered at 5 km, and became positive again only in the outflow layer. In the mean downshear sounding, large helicity again occurred in the boundary layer and outflow layers, but positive helicity also extended throughout the troposphere. The near-convection mean sounding (not shown) closely resembled the downshear mean, but was slightly larger at almost every level.

Figure 9a shows the vertical distribution of radial velocity for the mean upshear, downshear, and near-convection soundings. The differences were dramatic. Upshear soundings exhibited much weaker and shallower inflow in the lower troposphere, as well as weaker outflow aloft, than downshear soundings. The near-convection soundings contained mean inflow of 18 ms^{-1} just above the surface, and maximum outflow near the 6.5 km elevation. These differences matched those found by Zhu et al. (2004) and Cram et al. (2007). Tangential velocity (Fig 9b) varied as expected given the radial velocity: upshear soundings had weaker tangential velocity in the lower troposphere and larger tangential velocity in the middle and upper troposphere. The radial velocity variation in Figure 9a was consistent with the circulation induced by vertical wind shear (e.g., Franklin et al. 1993; Black et al. 2002). Downshear this results in stronger inflow in

the lower troposphere, stronger outflow above, and thus stronger clockwise turning. Upshear, the clockwise turning is much weaker because the shear-induced circulation opposes it. Although tropical cyclone response to shear is quite complex (e.g., Reasor et al. 2004; Cram et al. 2007), these simple arguments account broadly for the differences in wind profiles, and thus helicity, upshear and downshear of the center.

A kinematic description of helicity in the downshear soundings can be made using Eq 2. In the lower troposphere, helicity was large where positive tangential velocity multiplied a strong increase of radial velocity with height. In the upper troposphere the primary positive contribution arose from the remaining term in Eq 2, in which positive radial velocity multiplied a negative tangential velocity gradient with height.

It has been argued that the large helicity arose as a result of the response of the hurricane to vertical wind shear. It is also likely, however, that the large helicity enhances the in-up-out response downshear by producing long-lasting, intense cells. This in turn enhances clockwise turning and helicity. By this reasoning, large helicity might create a feedback that enhances the ability of the storm to resist wind shear.

The focus has been on the unusual helicity values in Hurricane Bonnie. But supercells and other local intense cells like the VHTs of Montgomery et al. (2006) require CAPE for their existence as well. The combined roles of CAPE and helicity will be addressed using two empirical indices. The first is the supercell composite parameter developed by Thompson et al. (2002), given by

$$SCP = (MUCAPE/1000\ J\ kg^{-1}) \times (SREH(0\text{-}3\ km)/100\ m^2\ s^{-2}) \times (BRN\ shear/40\ ms^{-1}) \qquad (4)$$

where MUCAPE is the most unstable CAPE and BRN shear is the magnitude of the vector difference between mass-weighted mean wind from 0-6 km and mass-weighted mean wind from

0-500m (e.g., Weisman and Klemp 1986). Thompson et al. (2002) defined SCP > 1 as favorable for supercell formation. The second empirical measure is the energy-helicity index (EHI; see, for instance, Davies 1993):

$$EHI = (MUCAPE/1600\ J\ kg^{-1})\ X\ (SREH(0\text{-}3\ km)/100\ m^2\ s^{-2}) \quad (5)$$

Rasmussen and Blanchard (1998) found median values of EHI for ordinary, supercell, and tornadic supercell convection in midlatitudes of 0.14, 0.64, and 1.48, respectively.

Table 3 shows MUCAPE, SREH, BRN shear, SCP, and EHI for the four soundings near deep convection in this study, plus two additional soundings upwind of the deep convection. Table 3 shows that despite the modest CAPE, supercell conditions were met for two of the four soundings nearest the deep cells. For the other two (D2 and D5), CAPE values of only 283 and 405 J kg^{-1}, respectively, would have been sufficient to make SCP > 1. EHI exceeded the median supercell sounding value of Rasmussen and Blanchard (1998) in three of the four soundings nearest the convection. In addition, sounding D12, upwind of the region where intense cells developed two hours afterward (Figure 5), met both supercell criteria. Both empirical indices indicated that large helicity offset modest CAPE to favor supercells in some parts of the storm.

6. Discussion

The helicity presented in this paper is cell-relative (Davies-Jones et al. 1990). The large observed values indicate that the structure of Hurricane Bonnie favored the growth of long-lived cells, primarily in the downshear left quadrant with respect to the ambient vertical wind shear vector. Intense cells grew in that quadrant on both days in the presence of large helicity.

Empirical supercell parameters indicated that helicity contributions supplemented moderate CAPE to produce values supportive of supercell development.

The following sequence of events is proposed. Hurricane Bonnie experienced a strong increase in vertical wind shear on 23 August (Figure 1). In response, enhanced in-up-out flow occurred downshear, and in-down-out flow upshear (Figure 9; see also Franklin et al. 1993; Black et al. 2002). As a direct result of this response, cell-relative helicity dramatically increased downshear (Figure 2). Downshear convection, already favored by the shear-induced circulation, became stronger and longer-lived as a result of the large helicity (Figures 4-5). It is hypothesized that the downshear cells contained large vorticity, consistent with what is expected in a large-helicity environment. It is further proposed that these cells organized upscale (Lilly 1986) to offset the influence of vertical shear and help maintain the vortex. This argument uses the concepts of Montgomery et al. (2006), in which spinup of a storm occurs via the upscale organization of vorticity within individual cells.

Although an *association* of large helicity and intense convection has been shown in this paper, there is insufficient evidence of the radar and vorticity structure of the cells to be certain that supercells were present. Nevertheless, several pieces of evidence, both direct and indirect, support the importance of helicity and the existence of supercells in the evolution of Hurricane Bonnie:

(i) Intense localized convective cells during the times of dropsonde observations in Hurricane Bonnie existed only in the vicinity of large helicity. Upshear of the storm on 23-25 August, where helicity was much smaller, intense convective structures did not develop.

(ii) Helicity maxima over 3, 6, and 12-km layers in Hurricane Bonnie were 1303, 1579, and 2576 $m^2 s^{-2}$, respectively. To the authors' knowledge, these values represent the largest

ever reported in the literature for each of the three layers. This indicates the likelihood of deep, long-lasting cells, whether or not the cells closely resemble their middle latitude counterparts.

(iii) Large environmental helicity occurred in the form of strongly curved, semi-circular hodographs. The latter maximize the ability of a cell to gain helicity from its environment. As a result, the observed cells almost certainly contained very large helicity, and thus strongly rotating updrafts.

(iv) Bluestein and Jain (1985) argued that in the presence of large environmental helicity, the most likely convective structures were isolated supercells and back-building squall lines. Isolated supercells appeared to develop on 25 August (Figure 5). Back-building behavior (and upscale organization as the eyewall became more complete) occurred on 23 August (Figure 4). This evidence indirectly supports the proposed parallels to middle latitude severe weather.

(v) Rogers et al. (2003) showed simulated radar images (their Figure 7) valid early on 25 August, and again for 26 August. On 25 August the convective cells were quasi-circular, despite the likely presence of a strong filamentation region just outside the radius of maximum winds (Rozoff et al. 2006). The apparent resistance of simulated convection to horizontal shearing on that day argues for large helicity (Lilly 1986). On 26 August, when helicity was much smaller (Table 1), simulated radar images showed strong filamentation (Rogers et al. 2003).

(vi) Black et al. (2002) found that individual cells in sheared tropical cyclones moved with orbital velocities 56-72% of the mean wind. Braun et al. (2006) found that their simulated eyewall vortices in Hurricane Bonnie moved at about 70% of the mean wind. Each argued

that these motions are consistent with the presence of vortex Rossby waves (Montgomery and Kallenbach 1997). Table A1 in the Appendix, however, shows that the supercell-based estimates of cell motion in this study produced values between 52 and 79% of the mean wind. This indicates that a supercell paradigm also seems to fit the speed of motion of convective cells in this storm.

The core of a mature tropical cyclone often exhibits a lack of strong convective elements (e.g., Jorgenson 1984; Molinari et al. 1994). Occasionally, however, convective cells with intense updrafts and extreme vertical extent appear in or near the eyewall. Such cells have the potential to dramatically alter the mass and wind fields of the storm (Black et al. 1986) and aid in the resistance of the storm to vertical wind shear. The results of this study suggest that these intense cells might resemble curved-hodograph supercells. Helicity provides a bulk parameter for identifying the location and likelihood of occurrence of such events.

The mechanisms proposed for the downshear convective maximum in tropical cyclones have typically been quite subtle, often involving small temperature differences and/or dry dynamics (e.g., Frank and Ritchie 2001; Reasor et al. 2004). Based on the results of this study, it is proposed that large helicity plays a major role in favoring strong convection downshear. The relationship between helicity and convection in tropical cyclones using dropsondes from multiple storms will be described in future work.

Acknowledgements. This work could not have been done without the efforts of the pilots, scientists, and other participants in CAMEX-3. In particular, Ramesh Kakar, Robbie Hood, Edward Zipser, and Gerald Heymsfield organized the efforts that led to the data collected in this study. We thank Kay Shelton, Carl Schreck, Jaclyn Frank, James Belanger, and an anonymous reviewer for their suggestions and careful reading of the manuscript. Gridded analyses from the

ECMWF were obtained from the National Center for Atmospheric Research, which is supported by the National Science Foundation (NSF). This work was supported by NASA Grant NNG05GR26G and NSF Grant ATM0418682.

APPENDIX

The sensitivity of calculated helicity values to estimates of cell motion are examined in this Appendix. All estimates assumed a rightward-moving, cyclonic cell, which would be favored in the cyclonic environment of a tropical cyclone. The large-helicity hodographs in this study are all clockwise-turning, which also favors right movers (e.g., Klemp 1978; Weisman and Klemp 1984). Four methods were used to estimate cell motion. The method of Maddox (1976) assumes that the cell moves with 75% of the mean wind from the surface to 200 mb, and 30º to the right of the mean wind. The method of Bunkers et al. (2000) contains a mean wind component (the vector average wind over the lowest 6 km) plus a shear-induced propagation. The latter is assumed to be 90º clockwise of the 0-6 km shear vector, and with a magnitude of 7.5 ms^{-1}. Ramsay and Doswell (2005) evaluated several estimates of cell motion, and proposed an adjustment of the Bunkers et al. (2000) method. They calculated the mean wind component over 8 km depth rather than 6 km, while keeping the same propagation component. The fourth estimate of cell motion follows that used by McCaul (1991): simply the mean wind over the lowest 6 km. McCaul (1991) argued that the actual helicity (if true cell motion were known) would be 20-50% higher than the estimate using the 6-km mean wind for the cell motion. Finally, total helicity was also calculated, equivalent to assuming a cell motion of zero.

Table A1 (below) shows for each method the mean upshear and downshear helicity, and the maximum helicity, over the 0-6 km layer. Results for other layers (not shown) produced the same relative variation. Also shown in Table A1 is the mean magnitude of the cell motion for each method for the downshear sondes only.

Table A1 shows that the various estimates for cell motion produced substantial quantitative variations in helicity, but the qualitative variation between upshear and downshear

was unchanged. In addition, if one omits the McCaul (1991) method, which is known to produce low estimates, it is apparent that the downshear values were exceptionally large.

Table A1 shows for downshear soundings a nearly one-to-one variation between mean cell motion speed and helicity, with larger cell motions producing smaller helicity. Nearly all of the downshear soundings are strongly clockwise turning. Davies-Jones (1984) showed that helicity is proportional to the area swept out on a hodograph by the vector ***v-c.*** For a clockwise turning hodograph, this area is largest when |***v-c***| is largest. Because ***c*** contains a mean wind component, the two vectors have a component in common along the mean wind. As a result, the smaller the value of |***c***|, the larger the magnitude of ***v-c***, and the larger the value of helicity. This shows clearly for the downshear soundings, but not for the upshear soundings (not shown), which frequently do not display much clockwise turning.

One final estimate of cell motion was made from Rapid-Scan infrared images on 23 August. This provided an imperfect means of estimating cell motion because high clouds are advected and do not represent solely the motion of the cell. Nevertheless, when individual cells could be tracked over several consecutive images, they provided more information than the empirical estimates given above. These "observed" cell motions were calculated as follows: (i) Smooth the brightness temperatures from individual pixels using a 25-pixel (5 by 5 box) average; (ii) identify the location of the minimum brightness from consecutive images, and calculate a motion from those locations and the elapsed times using McIDAS software. This could be done only when unambiguous minima could be identified, and only during the 3 hours of Rapid Scans. Seven estimates were obtained, with an average speed of motion of 15.7 ms^{-1}. The motion was counterclockwise and outward. These rough estimates produced a smaller speed of cell motion than all of the methods above. Based on the reasoning of the previous paragraph, it is concluded

that the values used in the body of the paper did not overestimate the helicity, and might have underestimated it.

References

Black, M.L., R.W. Burpee, and F.D. Marks, Jr., 1996: Vertical motion characteristics of tropical cyclones determined with airborne Doppler radial velocities. *J. Atmos. Sci.*, **53**, 1887-1909.

Black, M.L., J.F. Gamache, F.D. Marks, Jr., C.E. Samsury, and H.E. Willoughby, 2002: Eastern Pacific hurricanes Jimena of 1991 and Olivia of 1994: The effect of vertical shear on structure and intensity. *Mon. Wea. Rev.,* **130**, 2291-2312.

Black, P.G., and F.D. Marks, Jr., 1987: Environmental interactions associated with hurricane supercells. Preprints, *17th Conf. on Hurricanes and Tropical Meteor.*, Amer. Meteor. Soc., Miami, FL, 22-26 Sept., 416-419.

Black, P.G., F.D. Marks, Jr., and R.A. Black, 1986: Supercell structure in tropical cyclones. *Proc. 23rd Conf. on Radar Meteor.*, Snowmass, CO, Amer. Meteor. Soc., JP255-259.

Bluestein, H.B., and M.H. Jain, 1985: Formation of mesoscale lines of precipitation: severe squall lines in Oklahoma during the spring. *J. Atmos. Sci.*, **42**, 1711-1732.

Bogner, P.B., G.M. Barnes, and J.L. Franklin, 2000: Conditional instability and shear for six hurricanes over the Atlantic Ocean. *Wea. Forecasting*, **15**, 192-207.

Brandes, E.A., R.P. Davies-Jones, and B.C. Johnson, 1988: Streamwise vorticity effects on supercell morphology and persistence. *J. Atmos. Sci.*, **45**, 947-963.

Braun, S.A., M.T. Montgomery, and Z. Pu, 2006: High-resolution simulation of Hurricane Bonnie (1998). Part I: The organization of eyewall vertical motion. *J. Atmos. Sci.*, **63**, 19-42.

Brooks, H.E., and R.B. Wilhelmson, 1993: Hodograph curvature and updraft intensity in numerically modeled supercells. *J. Atmos. Sci.*, **50**, 1824-1833.

Bunkers, M.J., B.A. Klimowski, J.W. Zeitler, R.L. Thompson, and M.L. Weisman, 2000: Predicting supercell motion using a new hodograph technique. *Wea. Forecasting*, **15**, 61-79.

Chen, S.S., J.A. Knaff, and F.D. Marks, Jr., 2006: Effects of vertical wind shear and storm motion on tropical cyclone rainfall asymmetries deduced from TRMM. *Mon. Wea. Rev.,* **134**, 3190-3208.

Corbosiero, K.L., and J. Molinari, 2002: The effects of vertical wind shear on the distribution of convection in tropical cyclones. *Mon. Wea. Rev.,* **130**, 2110-2123.

Corbosiero, K.L., and J. Molinari, 2003: The relationship between storm motion, vertical wind shear, and convective asymmetries in tropical cyclones. *J. Atmos. Sci.*, **60**, 366-376.

Cram, T.A., J. Persing, M.T. Montgomery, and S.A. Braun, 2007: A Lagrangian trajectory view on transport and mixing processes between the eye, eyewall, and environment using a high-resolution simulation of Hurricane Bonnie (1998). *J. Atmos. Sci.*, **64**, 1835-1856.

Davies, J.M., 1993: Hourly helicity, instability, and EHI in forecasting supercell tornadoes. Preprints, *17th Conf. on Severe Local Storms*, Kansas City, MO, Amer. Meteor. Soc., 107-111.

Davies-Jones, R.P., 1984: Streamwise vorticity: the origin of updraft rotation in supercell storms. *J. Atmos. Sci.*, **41**, 2991-3006.

Davies-Jones, R.P., D. Burgess, and M. Foster, 1990: Test of helicity as a tornado forecast parameter. Preprints, *16th Conf. Severe Local Storms*, Kanaskis, Alberta, CA, Amer. Meteor. Soc., 588-592.

Droegemeier, K.K., S.M. Lazarus, and R.P. Davies-Jones, 1993: The influence of helicity on numerically simulated convective storms. *Mon. Wea. Rev.*, **121**, 2005-2029.

Frank, W.M., and E.A. Ritchie, 2001: Effects of vertical wind shear on the intensity and structure of numerically simulated hurricanes**.** *Mon. Wea. Rev.*, **129**, 2249-2269.

Franklin, J.L., S.J. Lord, S.E. Feuer, and F.D. Marks, Jr., 1993: The kinematic structure of Hurricane Gloria (1985) determined from nested analyses of dropwindsonde and Doppler radar data. *Mon. Wea. Rev.*, **121**, 2433-2451.

Gentry, R.C., T.T. Fujita, and R.C. Sheets, 1970: Aircraft, spacecraft, satellite and radar observations of Hurricane Gladys, 1968: *J. Appl. Meteor.*, **9**, 837-850.

Hanley, D., J. Molinari, and D. Keyser, 2001: A composite study of the interactions between tropical cyclones and upper-tropospheric troughs. *Mon. Wea. Rev.*, **129**, 2570-2584.

Heymsfield, G.M., and Coauthors, 1996: The EDOP radar system on the high-altitude NASA ER-2 aircraft. *J. Atmos. Oceanic Technol*, **6**, 795-809.

Heymsfield, G.M., J. Halverson, E. Ritchie, J. Simpson, J. Molinari, and L. Yian, 2006: Structure of the highly sheared Tropical Storm Chantal during CAMEX-4. *J. Atmos. Sci.*, **63**, 268-287.

Heymsfield, G.M., J.B. Halverson, J. Simpson, L. Tian, and T.P. Bui, 2001: ER-2 Doppler radar investigations of the eyewall of Hurricane Bonnie during the Convection and Moisture Experiment-3. *J. Appl. Meteor.*, **40**, 1310-1330.

Johns, R.H., and C.A. Doswell III, 1992: Severe local storms forecasting. *Wea. Forecasting*, **7**, 588-612.

Jorgensen, D.P., 1984: Mesoscale and convective scale characteristics of mature hurricanes. Part II: Inner core structure of Hurricane Allen (1980). *J. Atmos. Sci.*, **41**, 1287-1311.

Jorgensen, D.P., E.J. Zipser, and M.A. LeMone, 1985: Vertical motions in intense hurricanes. *J. Atmos. Sci.*, **42**, 839-856.

Kakar, R., M. Goodman, R. Hood, and A. Guillory, 2006: Overview of the Convection and Moisture Experiment (CAMEX). *J. Atmos. Sci.*, **63**, 5-18.

Kerr, B.W., and G.L. Darkow, 1996: Storm-relative winds and helicity in the tornadic thunderstorm environment. *Wea. Forecasting*, **11**, 489-505.

Klemp, J.B., 1978: Simulations of right- and left-moving storms produced through storm splitting. *J. Atmos. Sci.*, **35**, 1097-1110.

Levich, E., and E. Tzvetkov, 1984: Helical cyclogenesis. *Phys. Lett.*, **100A**, 53-56.

Lilly, D.K., 1986: The structure, energetics, and propagation of rotating convective storms. Part II: Helicity and storm stabilization. *J. Atmos. Sci.*, **43**, 126-140.

Maddox, R.A., 1976: An evaluation of tornado proximity wind and stability data. *Mon. Wea. Rev.*, **104**, 133-142.

McCaul, E.W., Jr., 1987: Observations of the Hurricane "Danny" tornado outbreak of 16 August 1985. *Mon. Wea. Rev.*, **115**, 1206-1223.

McCaul, E.W., Jr., 1991: Buoyancy and shear characteristics of hurricane tornado environments. *Mon. Wea. Rev.*, **119**, 1954-1978.

McCaul, E.W., Jr., and M.L. Weisman, 1996: Simulations of shallow supercell storms in landfalling hurricane environments. *Mon. Wea. Rev.*, **124**, 408-429.

Molinari, J., P.K. Moore, V.P. Idone, R.W. Henderson, and A.B. Saljoughy, 1994: Cloud-to-ground lightning in Hurricane Andrew. *Journal of Geophysical Research*, **99**, 16,665-16,676.

Montgomery, M.T., M.E. Nicholls, T.A. Cram, and A.B. Saunders, 2006: A vertical hot tower route to tropical cyclogenesis. *J. Atmos. Sci.*, **63**, 355-386.

Montgomery, M. T., and R. J. Kallenbach, 1997: A theory for vortex Rossby waves and its application to spiral bands and intensity changes in hurricanes. *Quart. J. Roy. Meteor. Soc.*, **123**, 435-465.

Novlan, D.J., and W.M. Gray, 1974: Hurricane-spawned tornadoes. *Mon. Wea. Rev.*, **102**, 476-488.

Ramsay, H.A., and C.A. Doswell, 2005: A sensitivity study of hodograph-based methods for estimating supercell motion. *Wea. Forecasting*, **20**, 954-970.

Rasmussen, E.N., and D.O. Blanchard, 1998: A baseline climatology of sounding-derived supercell and tornado forecast parameters. *Wea. Forecasting*, **13**, 1148-1164.

Reasor, P.D., M.T. Montgomery, and L.D. Grasso, 2004: A new look at the problem of tropical cyclones in vertical shear flow: Vortex resiliency. *J. Atmos. Sci.*, **61**, 3-22.

Rogers, R., S. Chen, J. Tenerelli, and H. Willoughby, 2003: A numerical study on the impact of vertical shear on the distribution of rainfall in Hurricane Bonnie (1998). *Mon. Wea. Rev.*, **131**, 1577-1599.

Rozoff, C.M., W.H. Schubert, B.D. McNoldy, and J.P. Kossin, 2006: Rapid filamentation zones in intense tropical cyclones. *J. Atmos. Sci.*, **63**, 325-340.

Stiegler, D.J., and T.T. Fujita, 1982: A detailed analysis of the San Marcos, Texas, tornado induced by Hurricane Allen on 10 August 1980. Preprints, *12th Conf. Severe Local Storms*, San Antonio, TX, Amer. Meteor. Soc., 371-374.

Thompson, R.L., R. Edwards, and J.A. Hart, 2002: Evaluation and interpretation of the supercell composite and significant tornado parameters at the Storm Prediction Center. *21st Conf. on Severe Local Storms*, San Antonio, TX, Amer. Meteor. Soc., J11-J14.

Thompson, R.L., R. Edwards, J.A. Hart, K.L. Elmore, and P. Markowski, 2003: Close proximity soundings within supercell environments obtained from the Rapid Update Cycle. *Wea. Forecasting*, **18**, 1243-1261.

Weisman, M.L., and J.B. Klemp, 1982: The dependence of numerically simulated convective storms on vertical wind shear and buoyancy. *Mon. Wea. Rev.*, **110**, 504-520.

Weisman, M.L., and J.B. Klemp, 1984: The structure and classification of numerically simulated convective storms in directionally varying wind shears. *Mon. Wea. Rev.*, **112**, 2479-2498.

Weisman, M.L., and J.B. Klemp, 1986: Characteristics of isolated convective storms. *Mesoscale Meteorology and Forecasting*, P. Ray, Ed., Amer. Meteor. Soc., 331-358.

Weisman, M.L., and R. Rotunno, 2000: The use of vertical wind shear versus helicity in interpreting supercell dynamics. *J. Atmos. Sci.*, **57**, 1452-1472.

Wu, W.-S., D.K. Lilly, and R.M. Kerr, 1992: Helicity and thermal convection with shear. *J. Atmos. Sci.*, **49**, 1800-1809.

Zhu, T., D.-L. Zhang, and F. Weng, 2004: Numerical simulation of Hurricane Bonnie (1998). Part I: Eyewall evolution and intensity changes. *Mon. Wea. Rev.*, **132**, 225-241.

Figure Captions

Figure 1. Maximum surface wind (m s^{-1}; solid) and minimum central pressure (hPa; dashed) in Hurricane Bonnie from the Best Track data. Wind barbs show the ambient vertical wind shear between 850 and 200 hPa. Long barb = 5 ms^{-1}; short barb = 2.5 ms^{-1}. The shaded regions indicate the periods of dropsonde releases in the storm during CAMEX-3.

Figure 2. Dropsonde locations relative to the center of Hurricane Bonnie on 23-25 August, rotated with respect to the deep-layer vertical wind shear vector following Corbosiero and Molinari (2002). Downshear is toward the right. Two helicity values (m^2 s^{-2}) are plotted for each sounding: 0-6 km value (top number) and 0-3 km value (bottom number). In addition, the mean wind vector over the lowest 6 km is shown. The "D" numbers are labels for the dropsondes. Range rings are shown at 100 km intervals. The hurricane symbol represents the Best Track storm center. Wind barbs as in Figure 1.

Figure 3. As in Figure 2, but the numbers represent CAPE (J kg^{-1}) and the vectors represent the vertical wind shear vector over 6 km (5500-6000 m mean wind minus the 0-500 m mean wind).

Figure 4. Infrared satellite image at 2200 UTC 23 August, showing an intense local cell with a new cell forming upwind. The color bar represents brightness temperature in ºC. Helicity values and mean winds over 0-6 km from sondes D1-D6 (released between 1845 and 2136 UTC 23 August) are also shown, plotted with respect to the moving center. Vertical wind shear was from the northwest at this time. The hurricane symbol represents the Best Track center location.

Figure 5. As in Fig 4, but for 25 August at (a) 0100 UTC; (b) 0200 UTC; and (c) 0300 UTC. Helicity and 0-6 km mean winds from soundings taken between 2330 UTC 24 August and 0153 UTC 25 August are shown in (a). Vertical wind shear was from the west at this time.

Figure 6. Temperature (solid), dew point (dashed), and wind barbs for the four soundings nearest to the deep convective cells. The filled circle on the temperature sounding indicates the flight level from which each sonde was released. Temperatures between the first sonde level and 150 hPa were determined from a linear interpolation of potential temperature between the two levels. Values at and above 150 hPa were taken from ECMWF gridded analyses. Winds above flight level are from the same gridded analyses. (a) Sonde D2 at 1859 UTC 23 August; (b) D5 at 2119 UTC 23 August; (c) D9 at 2330 UTC 24 August; and (d) D10 at 2347 UTC 24 August.

Figure 7. Hodographs for the four soundings in Figure 6, plotted every 1 km in the vertical. The 1, 4, 7, and 10 km levels are labeled. Before plotting, a 1-2-1 smoother was applied in the vertical to the zonal and meridional winds. The hodograph for D5 in panel (b) begins at z = 200m; the remainder begin at z = 100m.

Figure 8. Vertical profiles of helicity (m^2 s^{-2}) in 1-km layers for the upshear (dashed) and downshear (solid) mean soundings.

Figure 9. Vertical distribution of radial [panel (a)] and tangential [panel (b)] velocities (m s^{-1}) averaged over the 7 upshear sondes (black), the 6 downshear sondes (red), and the 4 sondes nearest the deep cells (cyan).

TABLES

Table 1. Cell-relative environmental helicity over various layers (see Eq. 3), and local vertical wind shear from the surface to 6 km. The first three columns are from the midlatitude study of Thompson et al. (2003), who provided values only for the 0-3 km layer. The next three columns show the mean helicity from this study, averaged for regions with respect to the ambient vertical wind shear. These represent means of 7 sondes upshear of the center, 6 downshear, and 4 near deep convection, respectively. The final column on the right shows mean values for the 4 dropsondes on 26 August 1998, when environmental wind shear was much lower (see Figure 1).

U.S. MIDWEST (THOMPSON 2003)				HURRICANE BONNIE (1998)			
	Non-supercell	Non-tornadic supercell	Strong tornadic supercell	Upshear mean 8/23-25	Downshear mean 8/23-25	Near deep convection 8/23-25	Low env. shear mean 8/26
Helicity 0-3 km $m^2 s^{-2}$	49	180	250	177	520	748	201
Helicity 0-6 km $m^2 s^{-2}$	-	-	-	200	789	1017	250
Helicity 0-12 km $m^2 s^{-2}$	-	-	-	241	1276	1628	340
Vertical shear magnitude (m s^{-1}) 0-6 km	8	23	25	13	32	37	14

Table 2. Cell-relative environmental helicity over 3, 6, and 12 km layers (see Eq. 3), and local vertical wind shear magnitude between 0 and 6 km. The first two columns show values from the general tropical cyclone landfall and close tornado proximity soundings after landfall from McCaul (1991). The right three columns show helicity values from this study, averaged over the upshear and downshear halves and in the vicinity of deep convective cells as in Table 1, but using a different cell motion estimate (see Appendix) in order to be consistent with the McCaul (1991) values. This choice of cell motion significantly underestimates helicity (McCaul 1991; also see Appendix).

	McCaul (1991)		Hurricane Bonnie (1998)		
	General Hurricane landfall	Close tornado proximity	Upshear	Downshear	Near deep convective cells
Helicity 0-3 km $m^2 s^{-2}$	105	234	91	283	400
Helicity 0-6 km $m^2 s^{-2}$	138	330	99	422	563
Helicity 0-12 km $m^2 s^{-2}$	192	512	118	1076	1409
Vertical shear magnitude 0-6 km (m s^{-1})	10	14	13	32	37

Table 3. Values of the supercell composite parameter (SCP; Eq 4 in the text) of Thompson et al. (2002) and the energy-helicity index (EHI, Eq 5 in the text; see Davies 1993). Values are shown for the four soundings nearest the deep convective cells (soundings D2, D5, D9, and D10 in Figures 4 and 5) and for two soundings upstream of the deep cells (D12 and D13). Also shown are components of the indices: MUCAPE is most unstable CAPE in J kg^{-1}; SREH (m^2 s^{-2}) is helicity from Eq 3 of this paper; and BRN shear (ms^{-1}) is the magnitude of the vector difference between the mass-weighted mean wind from 0-6 km and the mass-weighted mean wind from 0-500m. Supercells are likely for SCP > 1. Supercell proximity soundings in midlatitudes contain a median EHI of 0.64 (Rasmussen and Blanchard 1998).

	MUCAPE J kg^{-1}	SREH(0-3 km) m^2 s^{-2}	BRN shear m s^{-1}	SCP	EHI
D2	218	776	18.2	0.77	1.06
D5	89	580	16.9	0.22	0.32
D9	1346	334	17.4	1.96	2.81
D10	792	1303	25.8	6.66	6.45
D12	1556	250	10.6	1.04	2.43
D13	1024	204	6.7	0.35	1.31

Table A1. Cell-relative helicity estimates ($m^2 s^{-2}$) for the 0-6 km layer. The average values for upshear and downshear sondes, and the maximum value (all for sonde D10), are shown, using four methods to obtain the cell motion. Total helicity was also calculated, equivalent to a cell motion of zero. The last column on the right shows the mean magnitude of the cell motion (m s^{-1}) for each method for the downshear sondes only.

Method to obtain the cell motion	Upshear mean helicity	Downshear mean helicity	Maximum helicity (sonde D10)	Mean $\|\boldsymbol{c}\|$ downshear
McCaul (1991)	99	422	1027	33
Bunkers et al 2000	190	677	1356	26
Ramsay and Doswell 2005 (see text)	200	789	1578	24
Maddox 1976	195	1146	2020	17
Total helicity	342	1586	2578	0

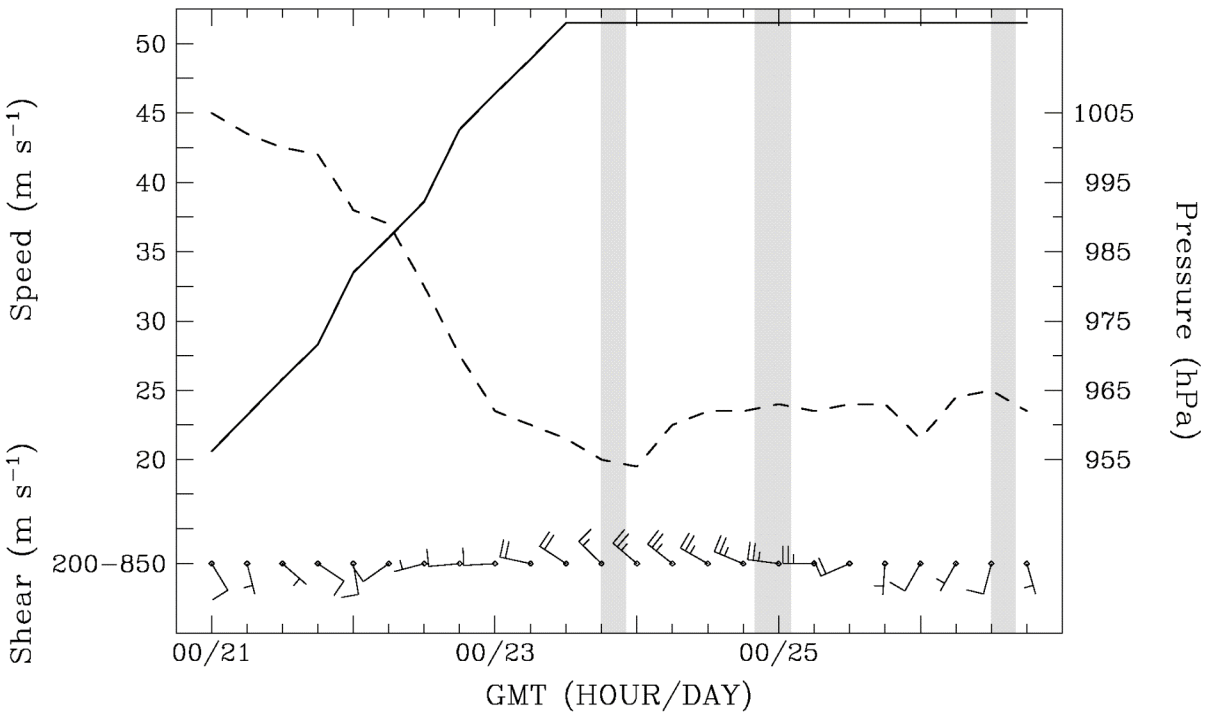

Figure 1. Maximum surface wind (m s^{-1}; solid) and minimum central pressure (hPa; dashed) in Hurricane Bonnie from the Best Track data. Wind barbs show the ambient vertical wind shear between 850 and 200 hPa. Long barb = 5 ms^{-1}; short barb = 2.5 ms^{-1}. The shaded regions indicate the periods of dropsonde releases in the storm during CAMEX-3.

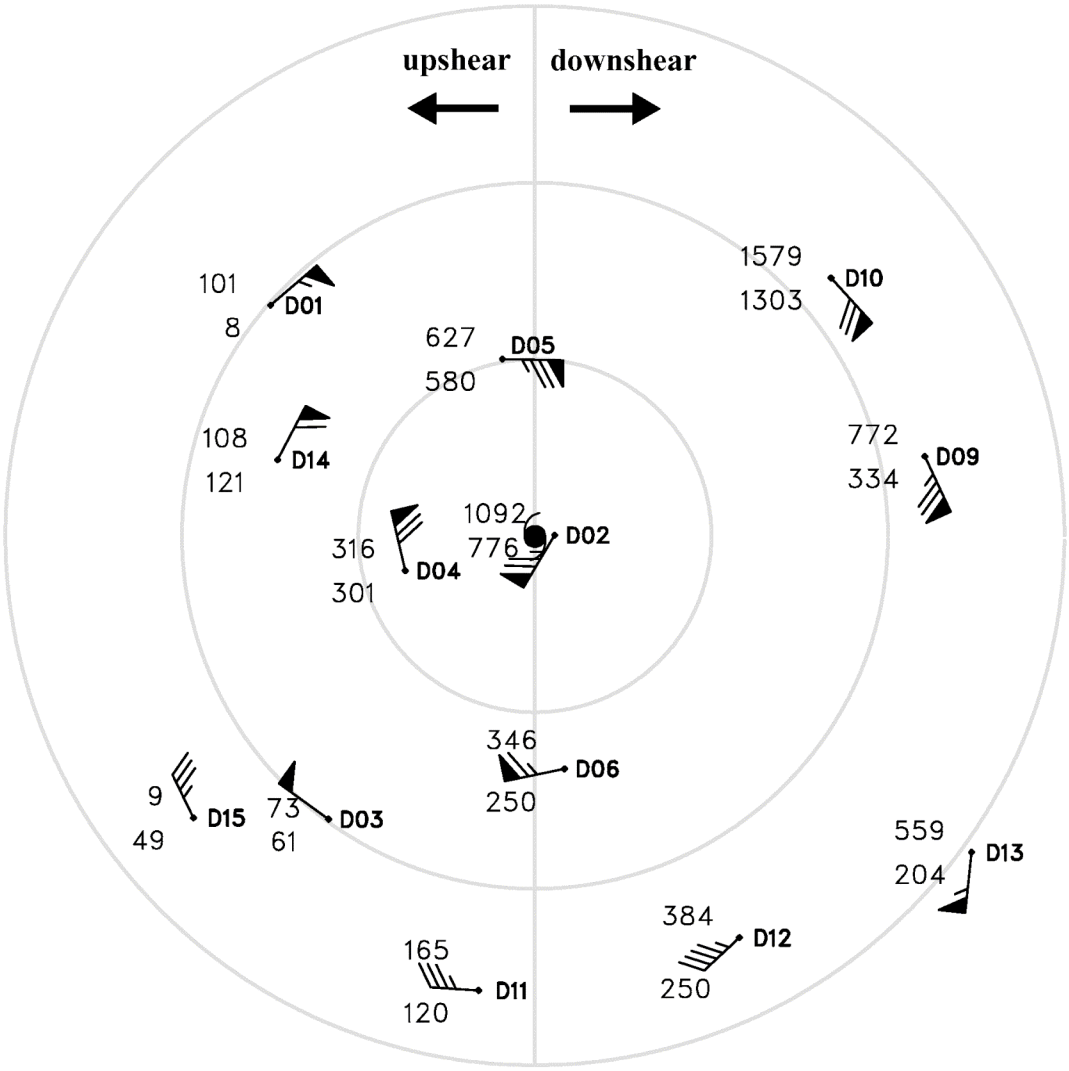

Figure 2. Dropsonde locations relative to the center of Hurricane Bonnie on 23-25 August, rotated with respect to the deep-layer vertical wind shear vector following Corbosiero and Molinari (2002). Downshear is toward the right. Two helicity values (m^2 s^{-2}) are plotted for each sounding: 0-6 km value (top number) and 0-3 km value (bottom number). In addition, the mean wind vector over the lowest 6 km is shown. The "D" numbers are labels for the dropsondes. Range rings are shown at 100 km intervals. The hurricane symbol represents the Best Track storm center. Wind barbs as in Figure 1.

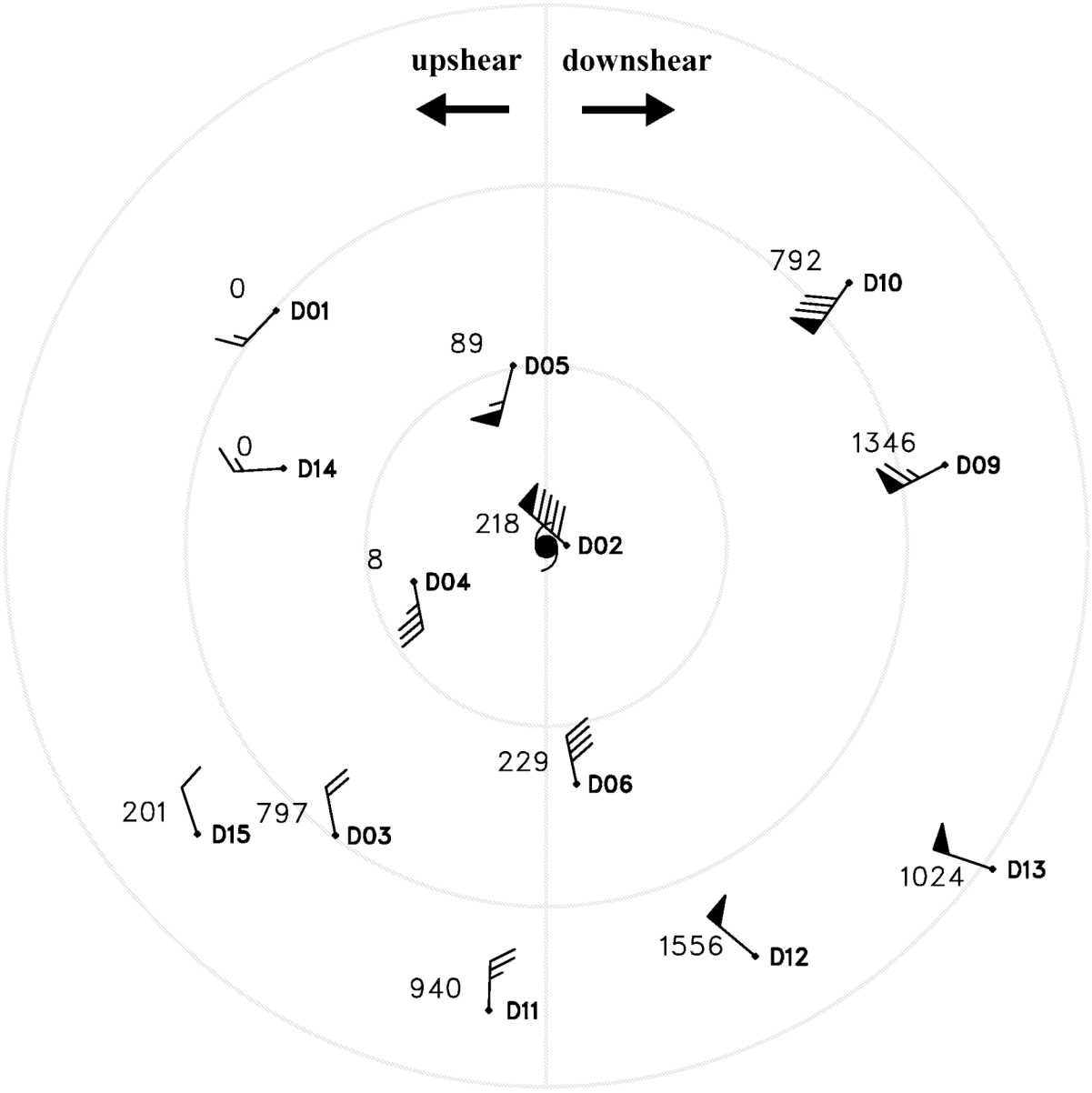

Figure 3. As in Figure 2, but the numbers represent CAPE (J kg^{-1}) and the vectors represent the vertical wind shear vector over 6 km (5500-6000 m mean wind minus the 0-500 m mean wind).

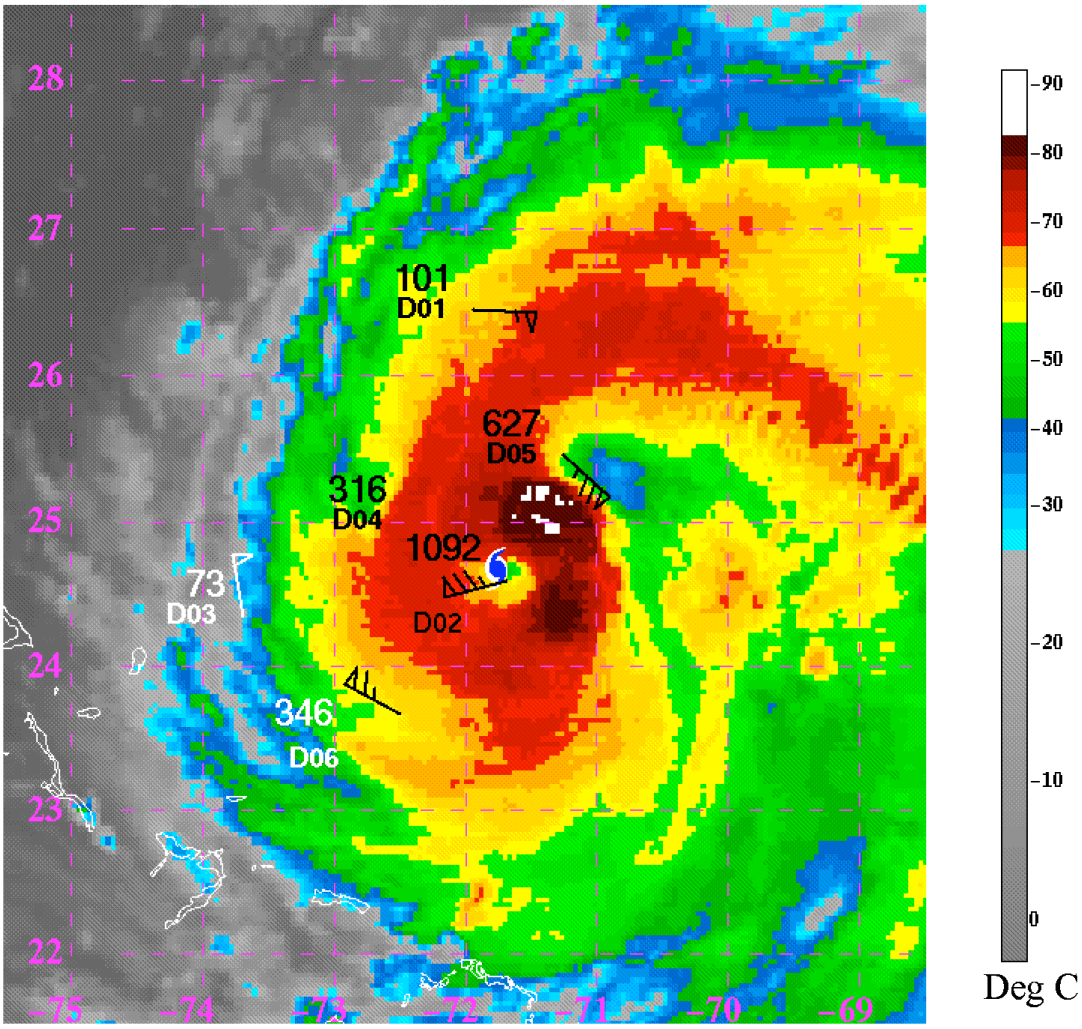

Figure 4. Infrared satellite image at 2200 UTC 23 August, showing an intense local cell with a new cell forming upwind. The color bar represents brightness temperature in ºC. Helicity values and mean winds over 0-6 km from sondes D1-D6 (released between 1845 and 2136 UTC 23 August) are also shown, plotted with respect to the moving center. These are shown in black or white depending upon the background. Vertical wind shear was from the northwest at this time. The hurricane symbol represents the Best Track center location.

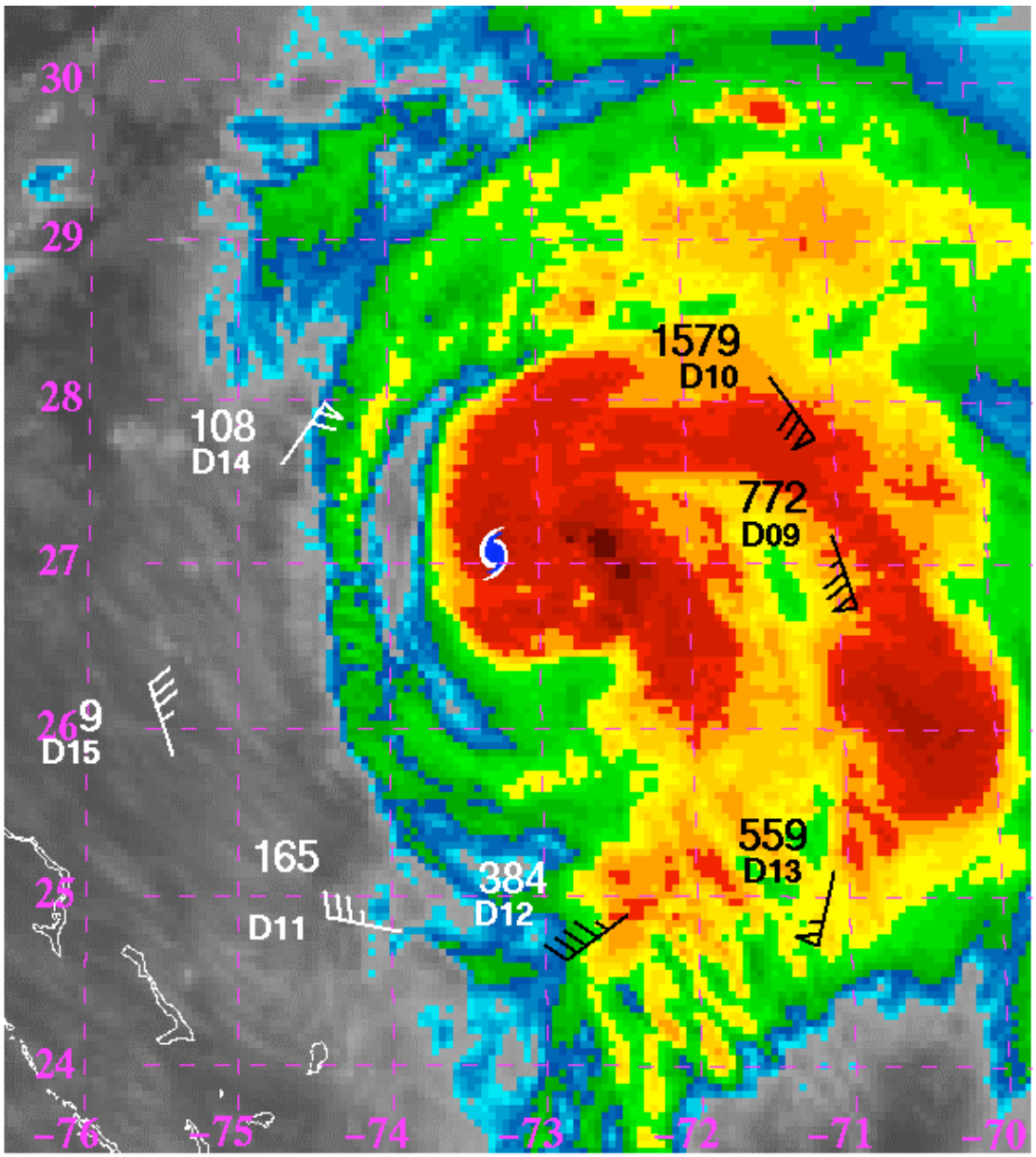

Figure 5. As in Fig 4, but for 25 August at (a) 0100 UTC; (b) 0200 UTC; and (c) 0300 UTC. Helicity and 0-6 km mean winds from soundings taken between 2330 UTC 24 August and 0153 UTC 25 August are shown in (a). Vertical wind shear was from the west at this time.

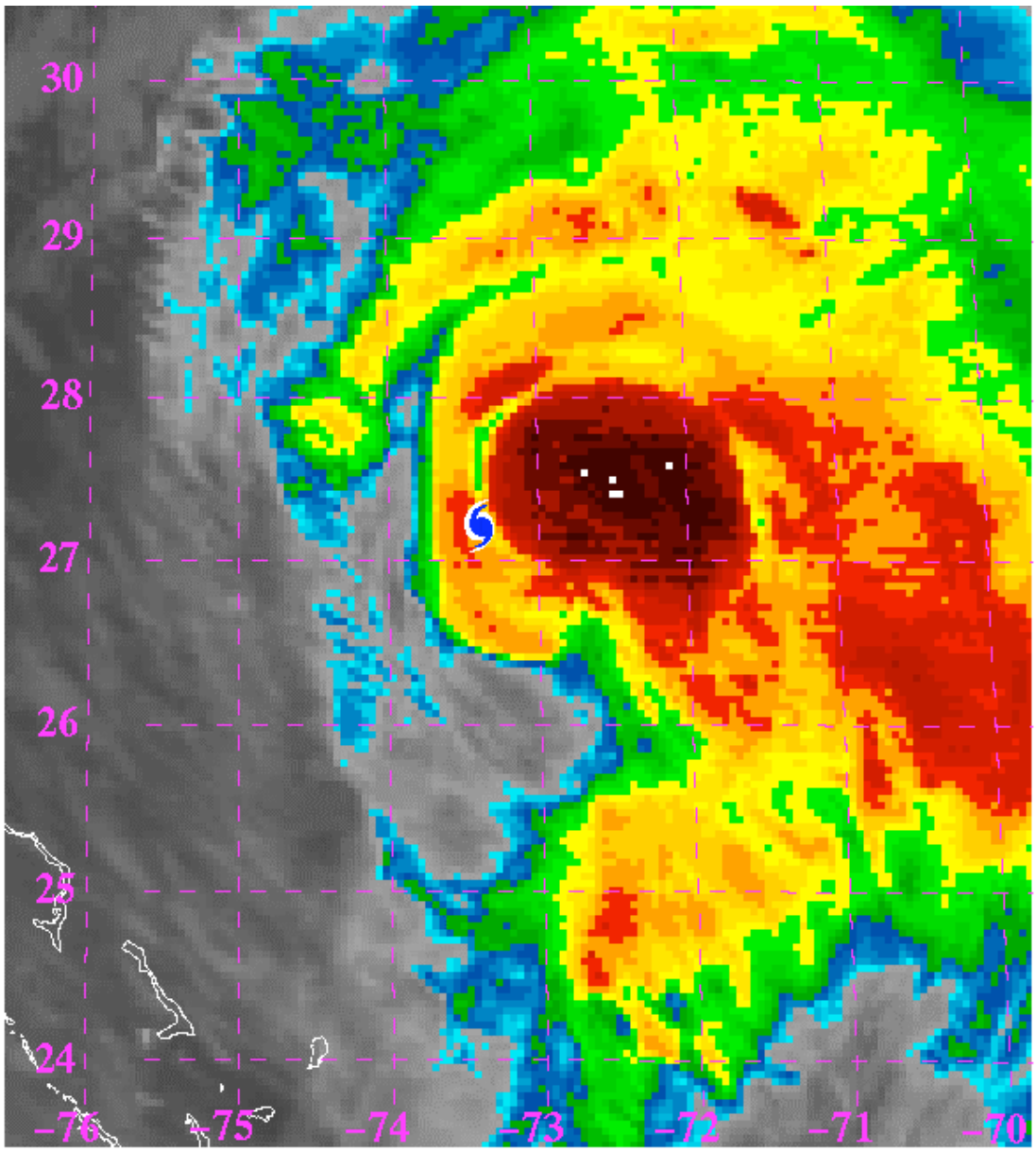

Figure 5b.

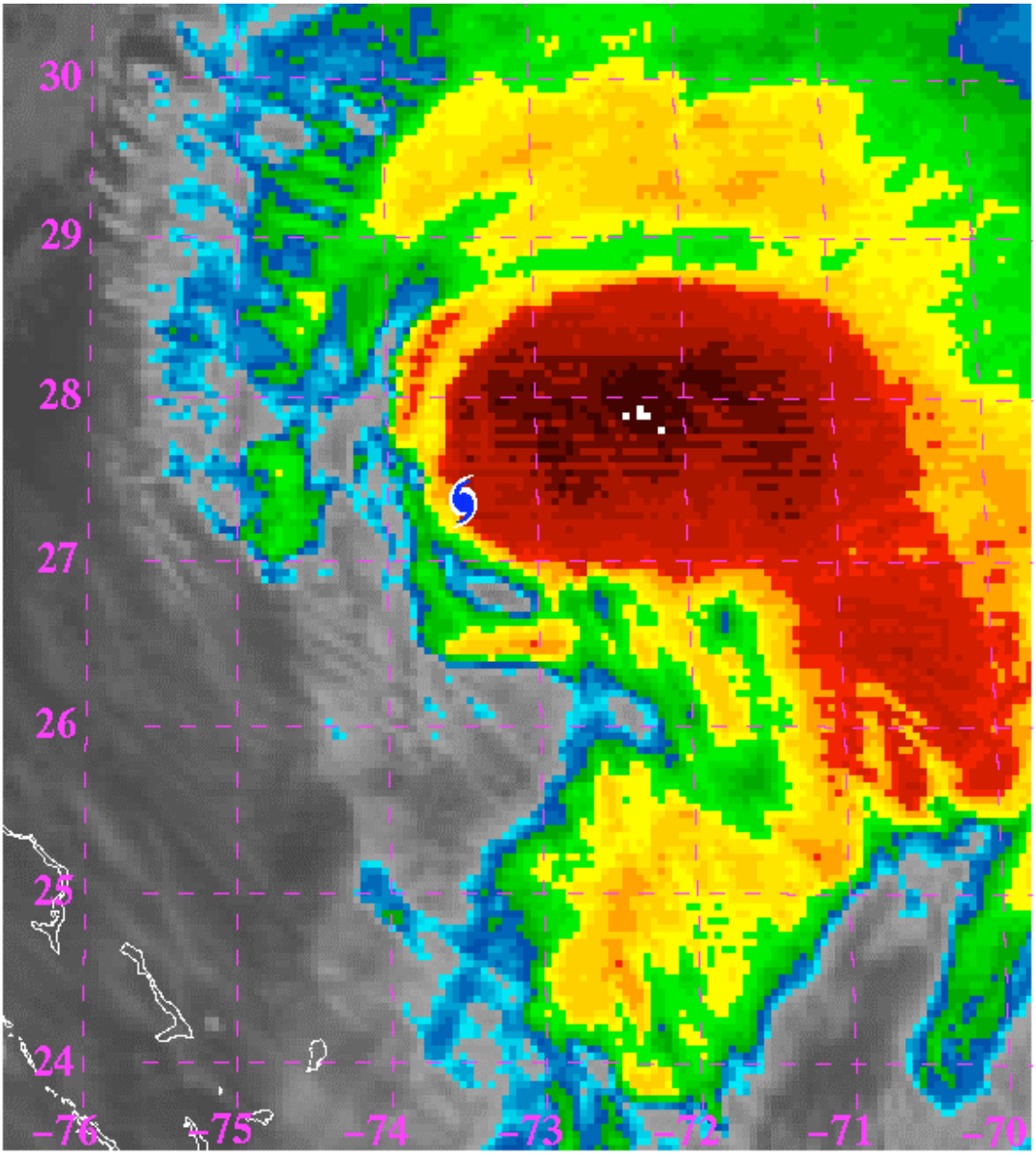

Figure 5c.

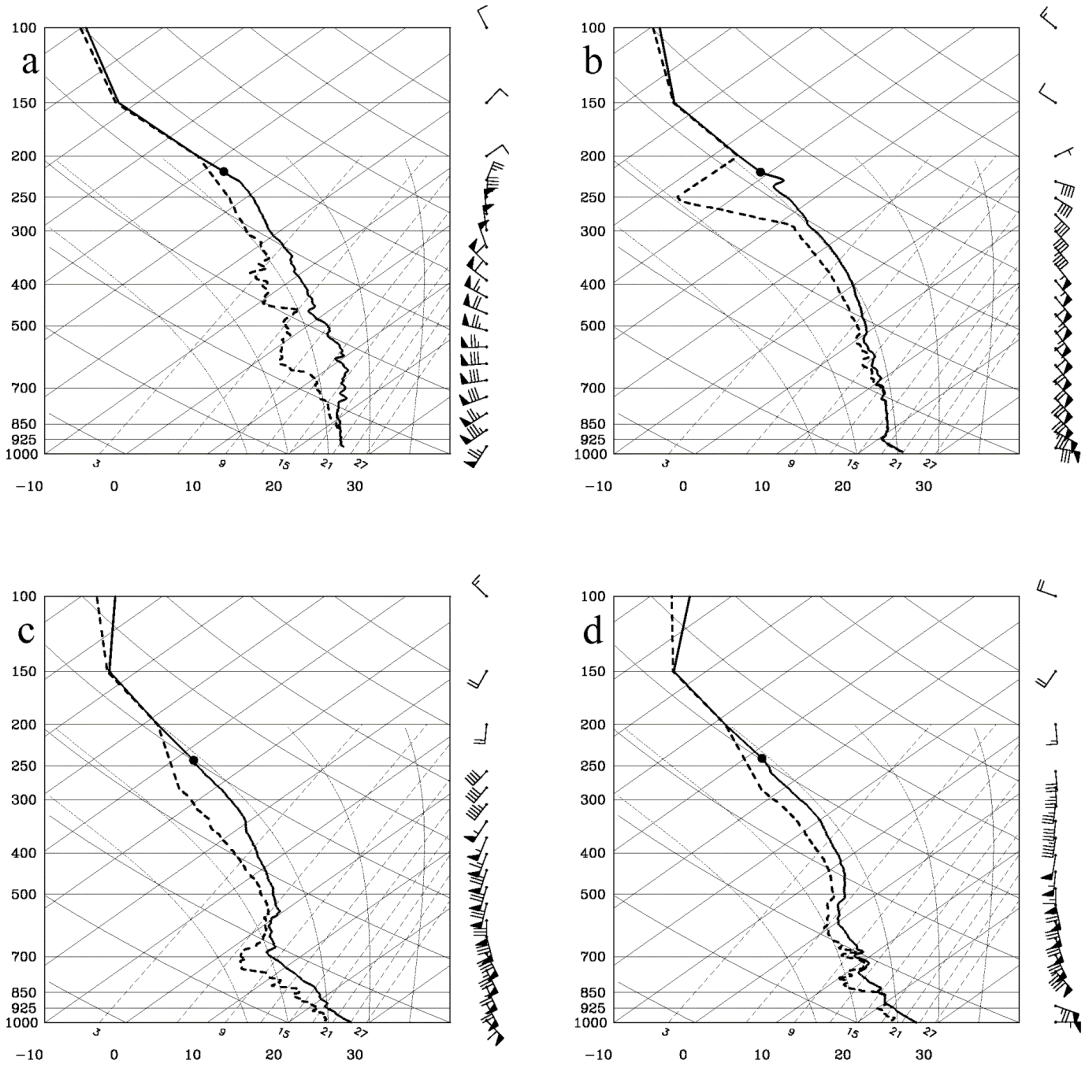

Figure 6. Temperature (solid), dew point (dashed), and wind barbs for the four soundings nearest to the deep convective cells. The closed circle on the temperature sounding indicates the flight level from which each sonde was released. Temperatures between the first sonde level and 150 hPa were determined from a linear interpolation of potential temperature between the two levels. Values at and above 150 hPa were taken from ECMWF gridded analyses. Winds above flight level are from the same gridded analyses. (a) Sonde D2 at 1859 UTC 23 August; (b) D5 at 2119 UTC 23 August; (c) D9 at 2330 UTC 24 August; and (d) D10 at 2347 UTC 24 August.

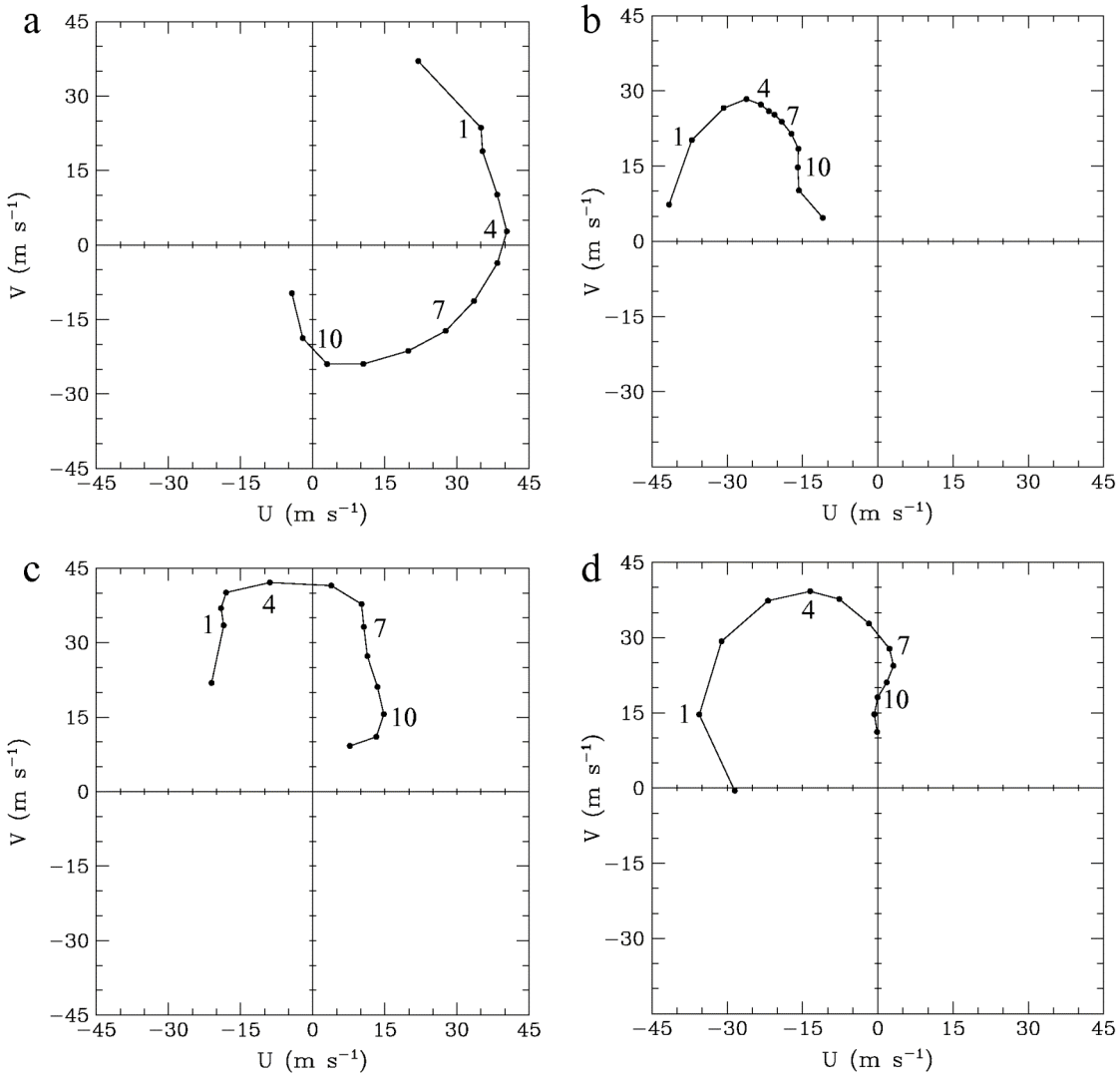

Figure 7. Hodographs for the four soundings in Figure 6, plotted every 1 km in the vertical. The 1, 4, 7, and 10 km levels are labeled. Before plotting, a 1-2-1 smoother was applied in the vertical to the zonal and meridional winds. The hodograph for D5 in panel (b) begins at z = 200m; the remainder begin at z = 100m.

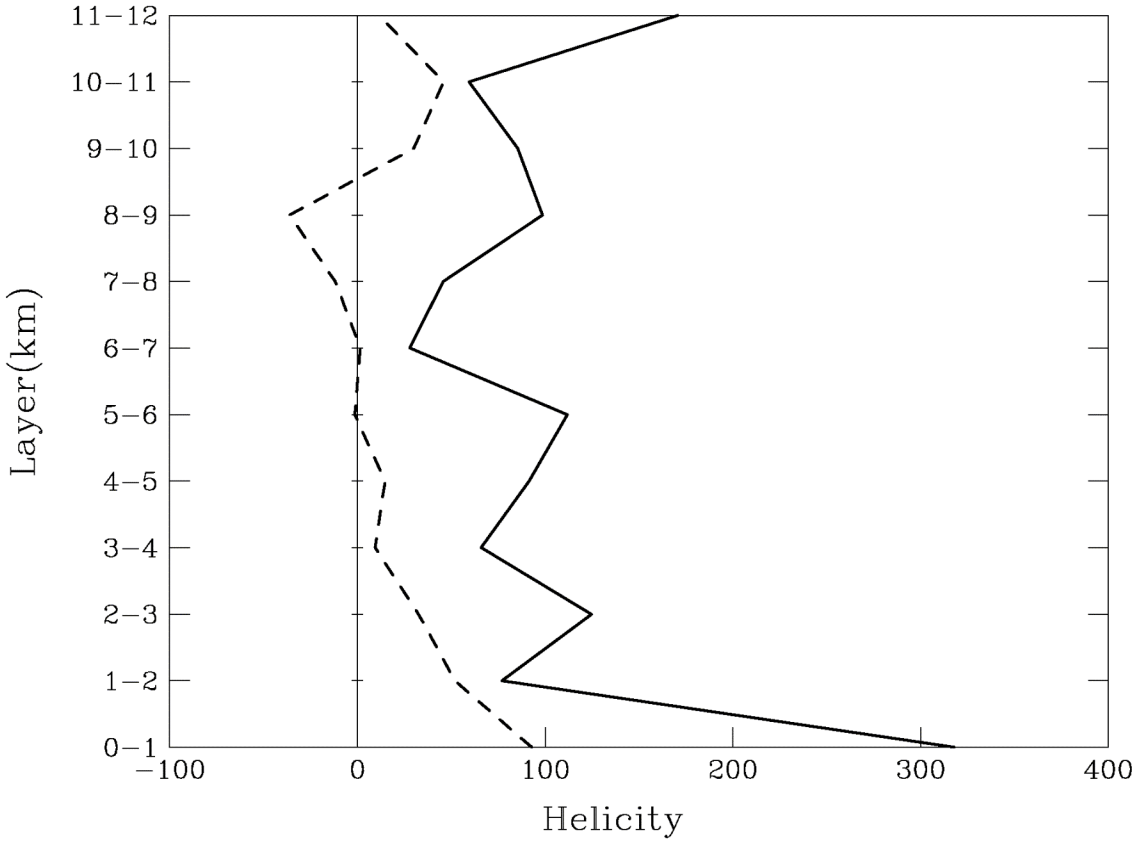

Figure 8. Vertical profiles of helicity (m^2 s^{-2}) in 1-km layers for the upshear (dashed) and downshear (solid) mean soundings.

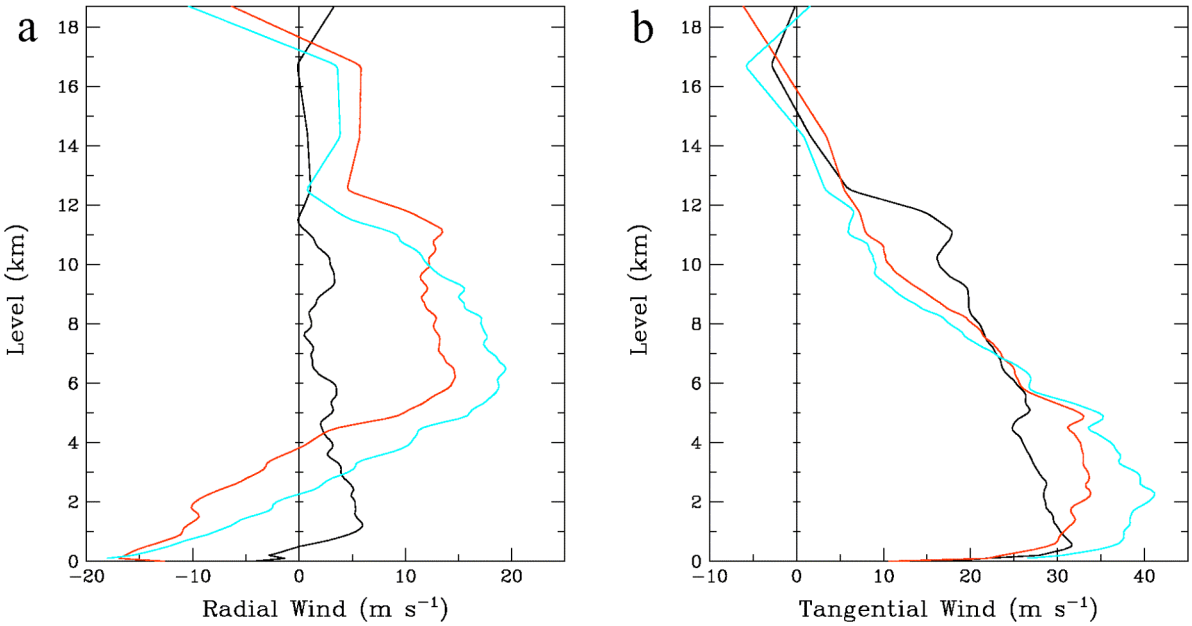

Figure 9. Vertical distribution of radial [panel (a)] and tangential [panel (b)] velocities (m s^{-1}) averaged over the 7 upshear sondes (black), the 6 downshear sondes (red), and the 4 sondes nearest the deep cells (cyan).